Zero-Bias Conductance Peaks Effectively Tuned by Gating-Controlled Rashba Spin-Orbit Coupling

Linhai Guo,[1,2] Yuedong Yan,[1,2] Rongge Xu,[3,4] Jian Li,[3,4,*] and Changgan Zeng[1,2,†]
[1]International Center for Quantum Design of Functional Materials (ICQD), Hefei National Laboratory for Physical Sciences at the Microscale, and Synergetic Innovation Center of Quantum Information and Quantum Physics, University of Science and Technology of China, Hefei, Anhui 230026, China
[2]CAS Key Laboratory of Strongly-Coupled Quantum Matter Physics, and Department of Physics, University of Science and Technology of China, Hefei, Anhui 230026, China
[3]Institute of Natural Sciences, Westlake Institute for Advanced Study, Hangzhou, Zhejiang 310024, China
[4]School of Science, Westlake University, Hangzhou, Zhejiang 310024, China

(Received 24 June 2020; revised 27 July 2020; accepted 23 December 2020; published 4 February 2021)

Zero-bias conductance peaks (ZBCPs) can manifest a number of notable physical phenomena and thus provide critical characteristics to the underlying electronic systems. Here, we report observations of pronounced ZBCPs in hybrid junctions composed of an oxide heterostructure $LaAlO_3/SrTiO_3$ and an elemental superconductor Nb, where the two-dimensional electron system (2DES) at the $LaAlO_3/SrTiO_3$ interface is known to accommodate gate-tunable Rashba spin-orbit coupling (SOC). Remarkably, the ZBCPs exhibit a domelike dependence on the gate voltage, which correlates strongly with the nonmonotonic gate dependence of the Rashba SOC in the 2DES. The origin of the observed ZBCPs can be attributed to the reflectionless tunneling effect of electrons that undergo phase-coherent multiple Andreev reflection, and their gate dependence can be explained by the enhanced quantum coherence time of electrons in the 2DES with increased momentum separation due to SOC. We further demonstrate theoretically that, in the presence of a substantial proximity effect, the Rashba SOC can directly enhance the overall Andreev conductance in the 2DES-barrier-superconductor junctions. These findings not only highlight nontrivial interplay between electron spin and superconductivity revealed by ZBCPs, but also set forward the study of superconducting hybrid structures by means of controllable SOC, which has significant implications in various research fronts from superconducting spintronics to topological superconductivity.

DOI: 10.1103/PhysRevLett.126.057701

The demonstration and characterization of zero-bias conductance peaks (ZBCPs) has played a crucial role in the investigations of a spectrum of physical effects, including Majorana bound states [1–10], Andreev bound states [11,12], reflectionless tunneling [13–22], weak antilocalization [23], Josephson effect [24], and Kondo resonance [25,26]. One most prominent example is the ZBCPs that signify the presence of Majorana bound states in normal-superconducting hybrid structures [1–8,27–29], where topological superconductivity can be induced owing to the proximity effect and strong spin-orbit coupling (SOC). In fact, the interplay between superconductivity and SOC is interesting in its own right [30–35]. The challenge to its in-depth study, however, lies in the difficulty to tune SOC effectively in hybrid structures. To circumvent this difficulty, a feasible and intriguing candidate is the oxide heterostructure $LaAlO_3/SrTiO_3$ (LAO/STO) [36–38], which hosts a two-dimensional electron system (2DES) at its interface. A well-known feature of such a 2DES is that the effective Rashba SOC therein can be tuned continuously with gate voltage (V_G) [39–45] and shows a domelike dependence on V_G, as has been observed through the measurement of weak antilocalization [43,45], superconducting critical magnetic field [45], and inverse Edelstein effect [44]. In this Letter, we exploit this nonmonotonic, gate-tunable SOC in a 2DES-barrier-superconductor (2DES/B/S) junction, where pronounced ZBCPs are observed and further discovered to correlate intimately with the SOC strength. A close analysis of this correlation reveals an effective tuning mechanism by the SOC on ZBCPs through phase-coherent multiple Andreev reflection [15–17].

As illustrated in Fig. 1(a), we performed four-point tunneling measurement on out-of-plane 2DES/B/S junctions composed of Nb and five unit-cell (001)-oriented LAO/STO (see Secs. 1 and 2 of the Supplemental Material [46]). The measured differential conductance spectra of sample No. 1 for various temperatures at $V_G = 0$ V are shown in Fig. 1(b). When the temperature is decreased below 7 K, a clear transport gap emerges as a consequence of the superconducting transition of the Nb electrode

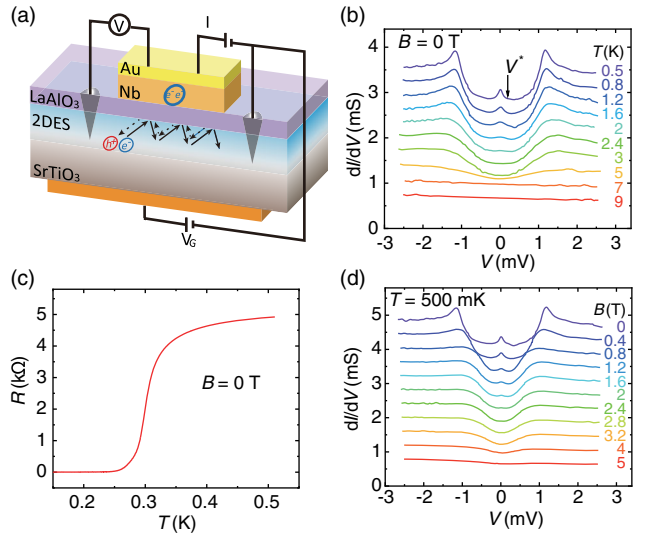

FIG. 1. (a) Schematic of an Nb/LAO/STO device for four-point tunneling measurements. The reflectionless tunneling process on the STO side is illustrated. (b) Tunneling spectra at different temperatures with $B = 0$ T. The characteristic bias voltage V^* for suppressing the reflectionless tunneling conductance is about 0.2 mV. (c) Temperature dependence of the 2DES resistance at $B = 0$ T. (d) Tunneling spectra at different parallel magnetic fields with $T = 500$ mK. All measurements were performed in Sample No. 1 at $V_G = 0$ V. Tunneling spectra in (b) and (d) are vertically shifted for clarity.

(see also Fig. S2 of the Supplemental Material [46]). Further deceasing the temperature to below a characteristic temperature $T^* \approx 2$ K, a ZBCP emerges in the superconducting gap and becomes more pronounced at lower temperature [Fig. 1(b)]. We note that this ZBCP may persist between the superconducting critical temperature (~300 mK) of the 2DES [Fig. 1(c)] and the superconducting critical temperature (~6.9 K) of the Nb electrode [see Fig. S2(a) of the Supplemental Material [46]], where the device is a well-defined normal-metal–barrier–superconductor (N/B/S) junction. The ZBCP becomes suppressed, however, by applying and gradually increasing magnetic field, as shown in Fig. 1(d).

A ZBCP in a tunneling experiment may have various possible origins, such as Kondo resonance [25,26], Andreev bound state [11], Majorana bound state [1–8, 27–29], weak antilocalization [23], Josephson effect [24], Ivanchenko-Zil'berman mechanism [57,58], and reflectionless tunneling [13–22]. By careful examination of each mechanism in our device, we rule out the first six possible origins listed above (see Sec. III of the Supplemental Material [46]), and attribute the observed ZBCP to the reflectionless tunneling between the normal-state 2DES and the superconducting Nb.

The reflectionless tunneling effect is a result of phase-coherent multiple Andreev reflections in N/B/S junctions [15–17]. In our 2DES/B/S junctions, the presence of the tunneling barrier generally favors the normal specular reflection of electrons from the 2DES while suppressing their Andreev reflection in a single scattering event. With a strong elastic backscattering in the junction, however, the normally reflected electrons can be scattered back to the superconducting interface, incurring additional and repeated Andreev reflection [see Fig. 1(a)]. When multiple Andreev reflection events interfere constructively, the overall probability of Andreev reflection is enhanced. This interference-led enhancement evidently depends on the energy and the dephasing time of the injected electrons and their partner holes—the maximum enhancement occurs at the Fermi level (zero energy), where the involved electrons and holes are related by time reversal symmetry; hence arises a ZBCP in the superconducting gap. The suppression of the Andreev differential conductance with increasing bias voltage defines a characteristic voltage V^* related to the Thouless energy of the 2DES: $E_{\mathrm{th}} = eV^* \approx 0.2$ meV [Fig. 1(b)] [15–17]. The dephasing temperature estimated from this Thouless energy, $T_{\mathrm{th}} = E_{\mathrm{th}}/k_B \approx 2.4$ K, is close to the observed characteristic temperature $T^* \approx 2$ K [Fig. 1(b)]. Moreover, by the Blonder-Tinkham-Klapwijk (BTK) fitting [59], we obtained the barrier parameter $Z \approx 2.44$, which gives a barrier transparency of $\Gamma_{\mathrm{N/B/S}} \approx 0.14$ (see detailed discussions in Sec. V of the Supplemental Material [46]). According to the previous theories and experiments about the reflectionless tunneling [16,17,21], a strong reflectionless tunneling effect can occur at such a barrier transparency, as observed in our experiments (Fig. 1). In addition, the response of the ZBCP to the magnetic field is also consistent with the reflectionless tunneling effect (see detailed discussions in Sec. VI of the Supplemental Material [46]). These cross-checks corroborate the reflectionless tunneling effect as a credible explanation for the ZBCP in our junctions.

Remarkably, the observed ZBCP exhibits a nontrivial gate tunability. The measured tunneling spectra at various V_G generally show an overall difference in the normal-state conductance G_N due to the change of carrier density in the 2DES [Fig. S7(a) of the Supplemental Material [46]]. In order to eliminate this relatively trivial contribution to the V_G dependence of our data, we normalized the tunneling spectra by G_N [see Fig. S7(b) of the Supplemental Material [46]], as has been widely practiced in previous studies [13,14,20,21]. The normalized tunneling spectra of sample No. 1 for different V_G at $T = 500$ mK are plotted in Figs. 2(a) and 2(b), and the corresponding normalized zero-bias conductance values are plotted in Fig. 2(c). The ZBCP exhibits a pronounced nonmonotonic V_G dependence, which becomes weaker with increasing temperature but survives even at 800 mK (Fig. S8 of the Supplemental Material [46]). We observed very similar features in sample No. 2, as shown in Figs. 2(d)–2(f). What is the origin of this domelike V_G dependence of ZBCP? We can exclude

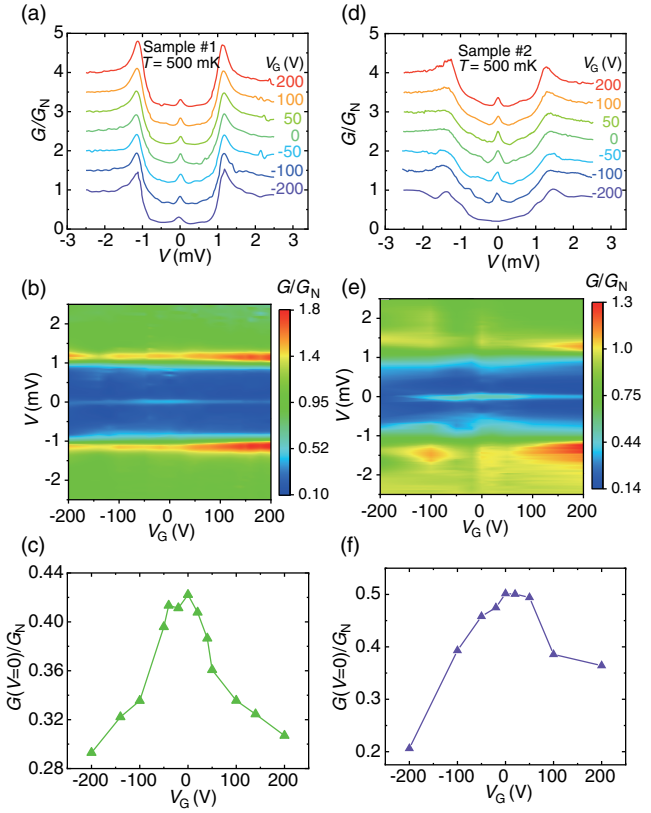

FIG. 2. (a),(b) Normalized tunneling spectra of sample No. 1 for different V_G at $T = 500$ mK. (c) Normalized zero-bias conductance as a function of V_G extracted from (a). (d),(e) Normalized tunneling spectra of sample No. 2 for different V_G at $T = 500$ mK. (f) Normalized zero-bias conductance as a function of V_G extracted from (d). All measurements were performed at $B = 0$ T. Tunneling spectra in (a) and (d) are vertically shifted for clarity.

several possibilities: first, it is obviously not from the nonmonotonic superconductivity of the 2DES [37], because the 2DES is in the normal state above 350 mK (Fig. S9 of the Supplemental Material [46]); second, the carrier density of the 2DES is monotonically dependent on V_G (Figs. S10 and S11 of the Supplemental Material [46]), and its effect has been eliminated after normalizing the tunneling spectra; third, the diffusion coefficient and the mobility are also monotonically dependent on V_G (Figs. S10 and S11 of the Supplemental Material [46]). In fact, the nonmonotonic V_G dependence of ZBCP is a clear reminiscence of the similarly behaved SOC in the 2DES [41–45], which we examine below.

We performed the magnetoresistance measurement of weak antilocalization in the 2DES to obtain the dependence of SOC on V_G in our samples. Figures 3(a) and 3(b) present the relative conductivity $\Delta\sigma = \sigma(B) - \sigma(0)$ of the 2DES as a function of perpendicular magnetic field at different V_G. Following previous studies [43,60,61], we adopted the Iordanskii, Lyanda-Geller, and Pikus (ILP) model to fit the experimental data (see detailed discussions in Sec. VII of the Supplemental Material [46]), and extracted the SOC energy Δ_{SO}, shown in Fig. 3(c) as a function of V_G. The SOC energy Δ_{SO} depends nonmonotonically on V_G, which is consistent with previous reports [41–45]. More importantly, we find that Δ_{SO} and ZBCP exhibit highly correlated V_G dependence with their maximal values both occurring at $V_G \approx 0$ V [Fig. 3(c)]. This suggests that the reflectionless tunneling effect might be effectively tuned by the SOC.

In order to gain further insight, we consider the SOC effect on the two key factors of reflectionless tunneling, namely the bare Andreev reflection probability and the decoherence rate in the N/B/S junction, respectively. The bare Andreev reflection probability concerns a single scattering event at the N/S interface, which can be modeled by the BTK theory [59]. As such, the Andreev reflection in a single scattering event will be determined by the wave function profile perpendicular to the 2DES, which in turn depends primarily on the confinement and the barrier potential but not on the Rashba SOC. The decoherence rate of electrons in the 2DES, on the other hand, can indeed depend on the SOC such that increased SOC may lead to enhanced reflectionless tunneling by suppressing phase decoherence scattering within the 2DES. We only consider the phase decoherence processes inside the 2DES by assuming that the tunneling time is much shorter than the phase coherence time in the 2DES, which is similar to previous studies of N/B/S junctions where the phase decoherence is considered in the N part only [13–22]. This mechanism can be explained as follows.

Figure 3(d) shows the band structure of the 2DES at the LAO/STO interface, which is calculated based on a three-band model of the t_{2g} conduction electrons [42]. The strongest Rashba SOC occurs at the avoided crossing point of d_{xy} subband and $d_{xz/yz}$ subband [Fig. 3(d)], where the splitting between the otherwise degenerate spin subbands also becomes maximal. Such a Rashba splitting can suppress the inelastic interband scattering at the Fermi surface significantly at low temperature. Explicitly, we consider the dominant dependence of the inelastic scattering rate on the SOC to be contributed by the interaction between electrons and acoustic phonons at low temperature [62–64], and find that to the leading order the inelastic interband scattering rate at the Fermi energy is given by $\Gamma_i \simeq \lambda k_B T[1 - 2\gamma(1 - \ln\gamma)]$, where λ and γ are both dimensionless; λ depends on the electron-phonon interaction strength and the acoustic phonon dispersion; $\gamma = (m^*\Delta_{SO}/2\hbar^2 q_c k_F)^2$ with k_F as the Fermi wave vector and q_c as the cutoff momentum for the acoustic phonon (we reasonably assume $\gamma \ll 1$ and $q_c \ll k_F$) (see Sec. VIII of the Supplemental Material [46]). As shown in Fig. 3(e), Γ_i decreases as Δ_{SO} increases, where the Δ_{SO} range is selected to be consistent with our experimental observations (1–3.5 meV) and previous studies (<10 meV) [38]. In other words, the dephasing time of electrons at the Fermi surface will be increased with stronger Rashba SOC, thus

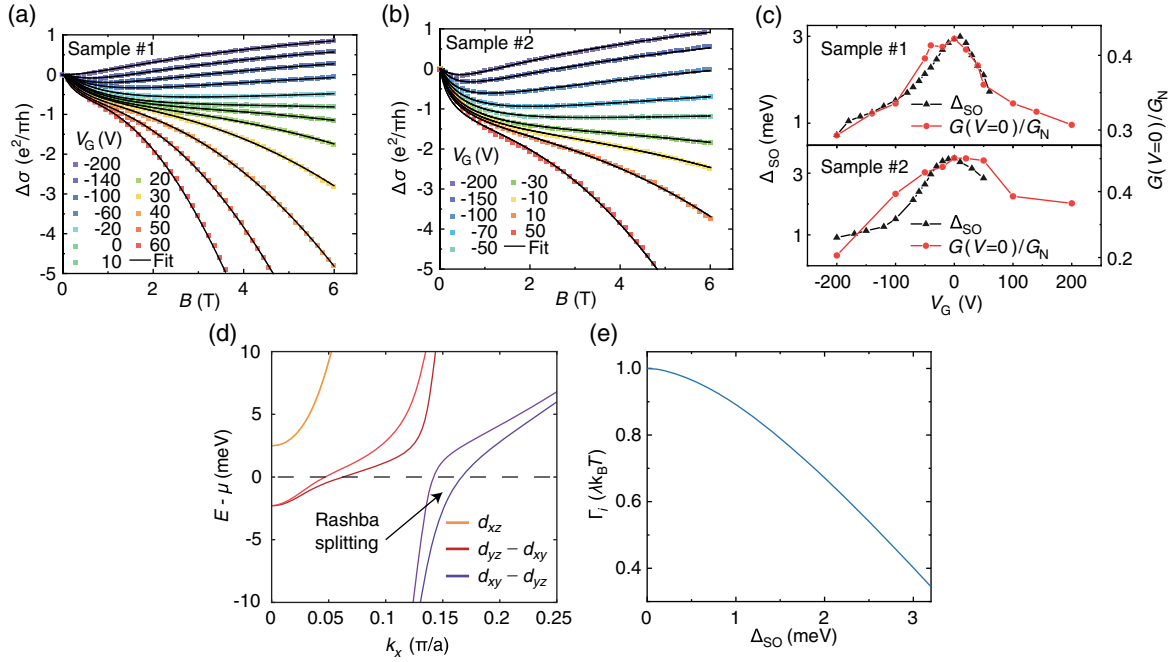

FIG. 3. (a),(b) Relative conductivity $\Delta\sigma$ as a function of perpendicular field for different V_G at $T = 1.5$ K (sample No. 1) and $T = 1.3$ K (sample No. 2), respectively. The black solid lines are the fits according to the ILP model. (c) V_G dependence of the spin-orbit energy Δ_{SO} (black triangles) extracted from the ILP fit and the normalized zero-bias conductance (red circles) extracted from Fig. 2. (d) Calculated band structure of the 2DES with SOC. (e) Inelastic interband scattering rate Γ_i as a function of Δ_{SO}. Here we estimate $k_F = 10^9$ m^{-1} and reasonably assume $q_c = 2 \times 10^8$ m^{-1} (see detailed discussions in Sec. VIII of the Supplemental Material [46]).

enhancing the ZBCP induced by the reflectionless tunneling, as observed experimentally [Fig. 3(c)].

The Rashba SOC leads to spin-dependent dispersion relations in the 2DES, but barely affect the Andreev reflection between the 2DES and the superconductor when the tunneling barrier is strong. This is, however, not the case in the opposite limit where the 2DES and the superconductor are strongly coupled to establish a sizable proximity effect. In the latter scenario, it is convenient to consider the Andreev reflection in an effectively in-plane fashion between the normal and the proximitized regions of the 2DES, as illustrated in Fig. 4(a). To investigate this scenario, we consider an alternative model composed of an in-plane 2DES/B/S junction as follows:

$$
\begin{aligned}
H = & \sum_{i_x,i_y,s} (4t - \mu) c^{\dagger}_{i_x,i_y,s} c_{i_x,i_y,s} \\
& + \sum_{i_x,i_y,s,s'} [(-t\sigma_0 - it_{\mathrm{SO}}\sigma_x)_{ss'} c^{\dagger}_{i_x,i_y+1,s} c_{i_x,i_y,s'} + \mathrm{H.c.}] \\
& + \sum_{i_x,i_y,s,s'} (1 - \eta\delta_{i_x 0})[(-t\sigma_0 + it_{\mathrm{SO}}\sigma_y)_{ss'} c^{\dagger}_{i_x+1,i_y,s} c_{i_x,i_y,s'} \\
& + \mathrm{H.c.}] + \sum_{i_x>0,i_y} (\Delta c^{\dagger}_{i_x,i_y,\uparrow} c^{\dagger}_{i_x,i_y,\downarrow} + \mathrm{H.c.}),
\end{aligned}
$$

where $c^{\dagger}_{i_x,i_y,s}$ is the creation operator for an electron at position (i_x, i_y) with spin s; μ and Δ are the chemical potential and the proximitized pairing parameter, respectively; $\eta \in [0, 1]$ represents the strength of the in-plane interfacial barrier; t and t_{SO} are the spin-independent hopping and the spin-orbit coupled hopping parameters, respectively. From the relation $k_{\mathrm{SO}} = \Delta_{\mathrm{SO}}/\hbar v_F = 2t_{\mathrm{SO}}/ta$, we convert t_{SO} to Δ_{SO}, $\Delta_{\mathrm{SO}} = 2\hbar^2 k_F t_{\mathrm{SO}}/tam^*$, where k_{SO} is the momentum splitting caused by the SOC at the Fermi level, v_F is the Fermi velocity, and a is the lattice constant assumed in our tight-binding model (note that a has nothing to do with the actual crystalline unit cell, but instead is taken as a discretization parameter for the long wavelength effective Hamiltonian). Based on this model, we calculated the differential Andreev conductance by using the well-established BTK method. In Fig. 4(b), we show the numerically obtained zero-bias differential Andreev conductance $G(V = 0)$, normalized by the normal-state ($\Delta = 0$) conductance G_N for the same setup, as a function of Δ_{SO} at various barrier strength η. We find a generic enhancement of $G(V = 0)/G_N$ with increasing Δ_{SO} in the experimentally observed range (1–3.5 meV). The mechanism behind this SOC-enhanced Andreev conductance can be understood by noticing that the SOC-led momentum splitting at the Fermi surface divides the Andreev scattering into two regimes depending on the transverse momentum (parallel to the interface) of the incoming state [see Fig. 4(c)]: if the transverse momentum involves both spin subbands, the Andreev scattering is prone to suppression by the interfacial barrier; if the transverse momentum involves only one spin

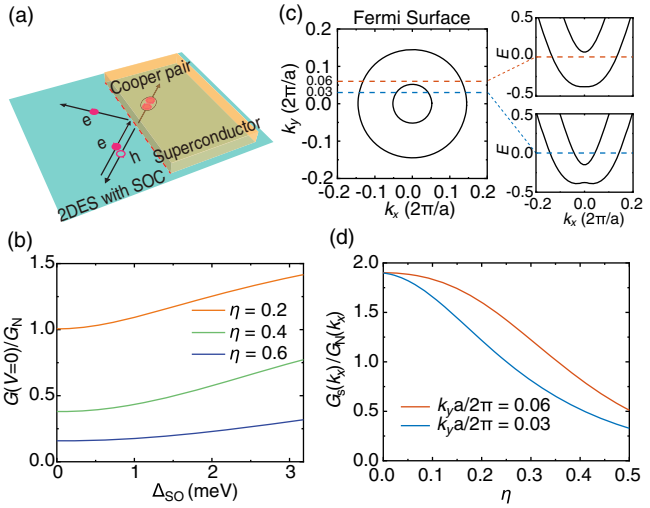

FIG. 4. (a) Andreev reflection at an in-plane 2DES/B/S junction interface. (b) Normalized zero-bias conductance as a function of Δ_{SO} for different interfacial barrier strength. Here we estimate $k_F = 10^9$ m^{-1} [46] and reasonably assume $a = 50$ nm. We set $\Delta/t = 0.02$ here and in (d). (c) Fermi surface and example band structure slices that illustrate the division of Andreev reflection into two scenarios depending on the number of scattering channels (Fermi points) at a specific transverse momentum k_y. (d) Normalized zero-bias conductance contributed by the two specific k_y in (c), as a function of barrier strength. We set $t_{SO}/t = 0.3$ in both (c) and (d).

subband, the Andreev scattering is more robust against the interfacial barrier [see Fig. 4(d)]. The contrast between these two regimes indeed represents a precursor of the enhanced Andreev reflection upon a topologically nontrivial chiral p-wave superconductor [30], where the Fermi surface involves exclusively a single spin-split subband (the second regime) because of additional breaking of time reversal symmetry. It follows that, with a sizable proximity effect, a larger momentum splitting due to increased SOC results in a larger Andreev conductance. Furthermore, this implies that, if the 2DES and the superconductor are strongly coupled, the ZBCP associated with the reflectionless tunneling can be tuned more straightforwardly by the SOC via its effect on the bare Andreev reflection probability.

In summary, we have observed ZBCPs that depend nonmonotonically on the gate voltage in 2DES/B/S junctions, where the 2DES and the tunneling barrier are produced by the LAO/STO heterostructure. Such a gate dependence can be attributed to the modulation of quantum phase coherence time, manifested through the reflectionless tunneling effect, by the gate-tuned SOC in the 2DES. Furthermore, we predict theoretically that, if the proximity effect becomes substantial due to strong coupling between the 2DES and the superconductor, the junction will generically exhibit enhanced Andreev conductance with increased Rashba SOC. This enhancement is a precursor of the onset of topological superconductivity, which is accompanied by Majorana fermion modes and robust Andreev reflection upon them [3]. Our results have not only discovered a nontrivial connection between SOC and quantum coherent transport characterized by ZBCPs, but have also paved a unique and systematic way toward engineered topological superconductivity with gate-controllable hybrid structures.

This work was supported in part by the National Natural Science Foundation of China (Grants No. 11974324 and No. 11774317), the Strategic Priority Research Program of CAS (Grant No. XDC07010000), the Anhui Initiative in Quantum Information Technologies (Grant No. AHY170000), and the Hefei Science Center CAS (Grant No. 2020HSC-UE014). This work was partially carried out at the USTC Center for Micro and Nanoscale Research and Fabrication.

L. G. and Y. Y. contributed equally to this work.

*Corresponding author.
lijian@westlake.edu.cn
†Corresponding author.
cgzeng@ustc.edu.cn

[1] A. Y. Kitaev, Unpaired Majorana fermions in quantum wires, Phys. Usp. **44**, 131 (2001).
[2] L. Fu and C. L. Kane, Superconducting Proximity Effect and Majorana Fermions at the Surface of a Topological Insulator, Phys. Rev. Lett. **100**, 096407 (2008).
[3] K. T. Law, P. A. Lee, and T. K. Ng, Majorana Fermion Induced Resonant Andreev Reflection, Phys. Rev. Lett. **103**, 237001 (2009).
[4] R. M. Lutchyn, J. D. Sau, and S. D. Sarma, Majorana Fermions and a Topological Phase Transition in Semiconductor-Superconductor Heterostructures, Phys. Rev. Lett. **105**, 077001 (2010).
[5] Y. Oreg, G. Refael, and F. Von Oppen, Helical Liquids and Majorana Bound States in Quantum Wires, Phys. Rev. Lett. **105**, 177002 (2010).
[6] V. Mourik, K. Zuo, S. M. Frolov, S. R. Plissard, E. P. Bakkers, and L. P. Kouwenhoven, Signatures of Majorana fermions in hybrid superconductor-semiconductor nanowire devices, Science **336**, 1003 (2012).
[7] S. Nadj-Perge, I. K. Drozdov, J. Li, H. Chen, S. Jeon, J. Seo, A. H. MacDonald, B. A. Bernevig, and A. Yazdani, Observation of Majorana fermions in ferromagnetic atomic chains on a superconductor, Science **346**, 602 (2014).
[8] H.-H. Sun, K.-W. Zhang, L.-H. Hu, C. Li, G.-Y. Wang, H.-Y. Ma, Z.-A. Xu, C.-L. Gao, D.-D. Guan, Y.-Y. Li, C. Liu, D. Qian, Y. Zhou, L. Fu, S.-C. Li, F.-C. Zhang, and J.-F. Jia, Majorana Zero Mode Detected with Spin Selective Andreev Reflection in the Vortex of a Topological Superconductor, Phys. Rev. Lett. **116**, 257003 (2016).
[9] D. Wang, L. Kong, P. Fan, H. Chen, S. Zhu, W. Liu, L. Cao, Y. Sun, S. Du, J. Schneeloch, R. Zhong, G. Gu, L. Fu, H. Ding, and H.-J. Gao, Evidence for Majorana bound states in an iron-based superconductor, Science **362**, 333 (2018).

[10] Q. Liu, C. Chen, T. Zhang, R. Peng, Y.-J. Yan, C.-H.-P. Wen, X. Lou, Y.-L. Huang, J.-P. Tian, X.-L. Dong, G.-W. Wang, W.-C. Bao, Q.-H. Wang, Z.-P. Yin, Z.-X. Zhao, and D.-L. Feng, Robust and Clean Majorana Zero Mode in the Vortex Core of High-Temperature Superconductor $(Li_{0.84}Fe_{0.16})$OHFeSe, Phys. Rev. X **8**, 041056 (2018).

[11] G. Deutscher, Andreev-Saint-James reflections: A probe of cuprate superconductors, Rev. Mod. Phys. **77**, 109 (2005).

[12] L. Bretheau, I. Joel, J. Wang, R. Pisoni, K. Watanabe, T. Taniguchi, and P. Jarillo-Herrero, Tunnelling spectroscopy of Andreev states in graphene, Nat. Phys. **13**, 756 (2017).

[13] A. Kastalsky, A. W. Kleinsasser, L. H. Greene, R. Bhat, F. P. Milliken, and J. P. Harbison, Observation of Pair Currents in Superconductor-Semiconductor Contacts, Phys. Rev. Lett. **67**, 3026 (1991).

[14] C. Nguyen, H. Kroemer, and E. L. Hu, Anomalous Andreev Conductance in InAs-AlSb Quantum Well Structures with Nb Electrodes, Phys. Rev. Lett. **69**, 2847 (1992).

[15] C. W. J. Beenakker, Quantum transport in semiconductor-superconductor microjunctions, Phys. Rev. B **46**, 12841 (1992).

[16] B. J. Van Wees, P. De Vries, P. Magne, and T. M. Klapwijk, Excess Conductance of Superconductor-Semiconductor Interfaces Due to Phase Conjugation between Electrons and Holes, Phys. Rev. Lett. **69**, 510 (1992).

[17] I. K. Marmorkos, C. W. J. Beenakker, and R. A. Jalabert, Three signatures of phase-coherent Andreev reflection, Phys. Rev. B **48**, 2811 (1993).

[18] P. H. C. Magnée, N. van der Post, P. H. M. Kooistra, B. J. van Wees, and T. M. Klapwijk, Enhanced conductance near zero voltage bias in mesoscopic superconductor-semiconductor junctions, Phys. Rev. B **50**, 4594 (1994).

[19] F. Giazotto, P. Pingue, F. Beltram, M. Lazzarino, D. Orani, S. Rubini, and A. Franciosi, Resonant Transport in Nb/GaAs/AlGaAs Heterostructures: Realization of the de Gennes-Saint-James Model, Phys. Rev. Lett. **87**, 216808 (2001).

[20] J. L. Dunford and A.-A. Dhirani, Reflectionless Tunneling at the Interface between Nanoparticles and Superconductors, Phys. Rev. Lett. **100**, 147202 (2008).

[21] A. Geresdi, A. Halbritter, and G. Mihály, Transition from coherent mesoscopic single-particle transport to Josephson proximity current, Phys. Rev. B **82**, 212501 (2010).

[22] H. Y. Günel, N. Borgwardt, I. E. Batov, H. Hardtdegen, K. Sladek, G. Panaitov, D. Grützmacher, and T. Schäpers, Crossover from Josephson effect to single interface Andreev reflection in asymmetric superconductor/nanowire junctions, Nano Lett. **14**, 4977 (2014).

[23] D. I. Pikulin, J. P. Dahlhaus, M. Wimmer, H. Schomerus, and C. W. J. Beenakker, A zero-voltage conductance peak from weak antilocalization in a Majorana nanowire, New J. Phys. **14**, 125011 (2012).

[24] A. Barone and G. Paterno, *Physics and Applications of the Josephson Effect* (Wiley, New York, 1982).

[25] T. A. Costi, Kondo Effect in a Magnetic Field, and the Magnetoresistivity of Kondo Alloys, Phys. Rev. Lett. **85**, 1504 (2000).

[26] Y. Yan, L. Guo, L. Li, L. Wei, W. Chen, C. Zeng, and J. Hou, Tuning the Kondo effect via gating-controlled orbital selection in the $LaAlO_3/SrTiO_3$ interfacial d-electron system, Phys. Rev. B **101**, 035119 (2020).

[27] P. W. Brouwer, M. Duckheim, A. Romito, and F. Von Oppen, Probability Distribution of Majorana End-State Energies in Disordered Wires, Phys. Rev. Lett. **107**, 196804 (2011).

[28] C. W. J. Beenakker, Search for Majorana fermions in superconductors, Annu. Rev. Condens. Matter Phys. **4**, 113 (2013).

[29] M. Sato and Y. Ando, Topological superconductors: A review, Rep. Prog. Phys. **80**, 076501 (2017).

[30] J. D. Sau, R. M. Lutchyn, S. Tewari, and S. D. Sarma, Generic New Platform for Topological Quantum Computation Using Semiconductor Heterostructures, Phys. Rev. Lett. **104**, 040502 (2010).

[31] L. P. Gor'kov and E. I. Rashba, Superconducting 2D System with Lifted Spin Degeneracy: Mixed Singlet-Triplet State, Phys. Rev. Lett. **87**, 037004 (2001).

[32] M. S. Scheurer and J. Schmalian, Topological superconductivity and unconventional pairing in oxide interfaces, Nat. Commun. **6**, 6005 (2015).

[33] W. Zhang and W. Yi, Topological Fulde-Ferrell-Larkin-Ovchinnikov states in spin-orbit-coupled Fermi gases, Nat. Commun. **4**, 2711 (2013).

[34] H. Yuan, M. S. Bahramy, K. Morimoto, S. Wu, K. Nomura, B.-J. Yang, H. Shimotani, R. Suzuki, M. Toh, C. Kloc, X. Xu, R. Arita, N. Nagaosa, and Y. Iwasa, Zeeman-type spin splitting controlled by an electric field, Nat. Phys. **9**, 563 (2013).

[35] Y. Xing, K. Zhao, P. Shan, F. Zheng, Y. Zhang, H. Fu, Y. Liu, M. Tian, C. Xi, H. Liu, J. Feng, X. Lin, S. Ji, X. Chen, Q.-K. Xue, and J. Wang, Ising superconductivity and quantum phase transition in macro-size monolayer $NbSe_2$, Nano Lett. **17**, 6802 (2017).

[36] A. Ohtomo and H. Y. Hwang, A high-mobility electron gas at the $LaAlO_3/SrTiO_3$ heterointerface, Nature (London) **427**, 423 (2004).

[37] A. D. Caviglia, S. Gariglio, N. Reyren, D. Jaccard, T. Schneider, M. Gabay, S. Thiel, G. Hammerl, J. Mannhart, and J.-M. Triscone, Electric field control of the $LaAlO_3/SrTiO_3$ interface ground state, Nature (London) **456**, 624 (2008).

[38] Y.-Y. Pai, A. Tylan-Tyler, P. Irvin, and J. Levy, Physics of $SrTiO_3$-based heterostructures and nanostructures: A review, Rep. Prog. Phys. **81**, 036503 (2018).

[39] A. D. Caviglia, M. Gabay, S. Gariglio, N. Reyren, C. Cancellieri, and J.-M. Triscone, Tunable Rashba Spin-Orbit Interaction at Oxide Interfaces, Phys. Rev. Lett. **104**, 126803 (2010).

[40] M. B. Shalom, M. Sachs, D. Rakhmilevitch, A. Palevski, and Y. Dagan, Tuning Spin-Orbit Coupling and Superconductivity at the $LaAlO_3/SrTiO_3$ Interface: A Magneto-transport Study, Phys. Rev. Lett. **104**, 126802 (2010).

[41] A. Joshua, S. Pecker, J. Ruhman, E. Altman, and S. Ilani, A universal critical density underlying the physics of electrons at the $LaAlO_3/SrTiO_3$ interface, Nat. Commun. **3**, 1129 (2012).

[42] M. Diez, A. M. R. V. L. Monteiro, G. Mattoni, E. Cobanera, T. Hyart, E. Mulazimoglu, N. Bovenzi, C. W. J. Beenakker, and A. D. Caviglia, Giant Negative Magnetoresistance Driven by Spin-Orbit Coupling at the $LaAlO_3/SrTiO_3$ Interface, Phys. Rev. Lett. **115**, 016803 (2015).

[43] H. Liang, L. Cheng, L. Wei, Z. Luo, G. Yu, C. Zeng, and Z. Zhang, Nonmonotonically tunable Rashba spin-orbit coupling by multiple-band filling control in $SrTiO_3$-based interfacial d-electron gases, Phys. Rev. B **92**, 075309 (2015).

[44] E. Lesne, Y. Fu, S. Oyarzun, J. C. Rojas-Snchez, D. C. Vaz, H. Naganuma, G. Sicoli, J.-P. Attan, M. Jamet, E. Jacquet, J.-M. George, A. Barthlmy, H. Jaffrs, A. Fert, M. Bibes, and L. Vila, Highly efficient and tunable spin-to-charge conversion through Rashba coupling at oxide interfaces, Nat. Mater. **15**, 1261 (2016).

[45] P. K. Rout, E. Maniv, and Y. Dagan, Link between the Superconducting Dome and Spin-Orbit Interaction in the (111) $LaAlO_3/SrTiO_3$ Interface, Phys. Rev. Lett. **119**, 237002 (2017).

[46] See Supplemental Material at http://link.aps.org/supplemental/10.1103/PhysRevLett.126.057701 for experimental and theoretical details, as well as additional figures and discussions, which includes Refs. [47–56].

[47] C. Richter, H. Boschker, W. Dietsche, E. Fillis-Tsirakis, R. Jany, F. Loder, L. F. Kourkoutis, D. A. Muller, J. R. Kirtley, C. W. Schneider, and J. Mannhart, Interface superconductor with gap behaviour like a high-temperature superconductor, Nature (London) **502**, 528 (2013).

[48] A. G. Swartz, H. Inoue, T. A. Merz, Y. Hikita, S. Raghu, T. P. Devereaux, S. Johnston, and H. Y. Hwang, Polaronic behavior in a weak-coupling superconductor, Proc. Natl. Acad. Sci. U.S.A. **115**, 1475 (2018).

[49] A. G. Swartz, A. K. C. Cheung, H. Yoon, Z. Chen, Y. Hikita, S. Raghu, and H. Y. Hwang, Superconducting Tunneling Spectroscopy of Spin-Orbit Coupling and Orbital Depairing in Nb:$SrTiO_3$, Phys. Rev. Lett. **121**, 167003 (2018).

[50] J. Bardeen, L. N. Cooper, and J. R. Schrieffer, Theory of superconductivity, Phys. Rev. **108**, 1175 (1957).

[51] A. Plecenník, M. Grajcar, Š. Beňačka, P. Seidel, and A. Pfuch, Finite-quasiparticle-lifetime effects in the differential conductance of $Bi_2Sr_2CaCu_2O_y$/Au junctions, Phys. Rev. B **49**, 10016 (1994).

[52] M. Basletic, J.-L. Maurice, C. Carrétéro, G. Herranz, O. Copie, M. Bibes, É. Jacquet, K. Bouzehouane, S. Fusil, and A. Barthélémy, Mapping the spatial distribution of charge carriers in $LaAlO_3/SrTiO_3$ heterostructures, Nat. Mater. **7**, 621 (2008).

[53] N. Reyren, S. Gariglio, A. D. Caviglia, D. Jaccard, T. Schneider, and J.-M. Triscone, Anisotropy of the superconducting transport properties of the $LaAlO_3/SrTiO_3$ interface, Appl. Phys. Lett. **94**, 112506 (2009).

[54] G. Bergmann, Weak localization in thin films: a time-of-flight experiment with conduction electrons, Phys. Rep. **107**, 1 (1984).

[55] L. F. Mattheiss, Effect of the 110°K phase transition on the $SrTiO_3$ conduction bands, Phys. Rev. B **6**, 4740 (1972).

[56] G. D. Mahan, *Many-Particle Physics*, 3rd ed. (Springer, New York, 2000).

[57] Y. M. Ivanchenko and L. A. Zil'Berman, The Josephson effect in small tunnel contacts, Sov. Phys. JETP **28**, 1272 (1969).

[58] W. Yu, R. Haenel, M. A. Rodriguez, S. R. Lee, F. Zhang, M. Franz, D. I. Pikulin, and W. Pan, Zero-bias conductance peak in Dirac semimetal-superconductor devices, Phys. Rev. Research **2**, 032002(R) (2020).

[59] G. E. Blonder, M. Tinkham, and T. M. Klapwijk, Transition from metallic to tunneling regimes in superconducting microconstrictions: Excess current, charge imbalance, and supercurrent conversion, Phys. Rev. B **25**, 4515 (1982).

[60] S. V. Iordanskii, Y. B. Lyanda-Geller, and G. E. Pikus, Weak localization in quantum wells with spin-orbit interaction, JETP Lett. **60**, 206 (1994).

[61] H. Nakamura, T. Koga, and T. Kimura, Experimental Evidence of Cubic Rashba Effect in an Inversion-Symmetric Oxide, Phys. Rev. Lett. **108**, 206601 (2012).

[62] J. L. Skinner, Theory of pure dephasing in crystals, Annu. Rev. Phys. Chem. **39**, 463 (1988).

[63] M. Bernardi, First-principles dynamics of electrons, and phonons, Eur. Phys. J. B **89**, 239 (2016).

[64] J.-J. Zhou, O. Hellman, and M. Bernardi, Electron-Phonon Scattering in the Presence of Soft Modes and Electron Mobility in $SrTiO_3$ Perovskite from First Principles, Phys. Rev. Lett. **121**, 226603 (2018).